Tethered surfaces: Statics and dynamics

Yacov Kantor

Department of Physics, Harvard University, Cambridge, Massachusetts 02138

Mehran Kardar

Department of Physics, Massachusetts Institute of Technology, Cambridge, Massachusetts 02139

David R. Nelson

Department of Physics, Harvard University, Cambridge, Massachusetts 02138

We apply renormalization-group and Monte Carlo methods to study the equilibrium conformations and dynamics of two-dimensional surfaces of fixed connectivity embedded in d dimensions, as exemplified by hard spheres tethered together by strings into a triangular net. A continuum description of the surfaces is obtained. Without self-avoidance, the radius of gyration increases as $\sqrt{\ln L}$, where L is the linear size of the uncrumpled surface. The upper critical dimension of self-avoiding surfaces is infinite. Their radius of gyration grows as L^{ν}, where Flory theory predicts $\nu = 4/(d+2)$, in agreement with our Monte Carlo result $\nu = 0.80 \pm 0.05$ in $d = 3$. The Rouse relaxation time of a self-avoiding surface grows as $L^{3.6}$.

I. INTRODUCTION

The large number of papers, reviews, and other publications testify to the growing importance of polymer research during the past few decades.[1] A linear polymer can be regarded as a one-dimensional manifold in a three-dimensional space. It is then natural to inquire into the behavior of two-dimensional manifolds embedded in higher-dimensional space, and in this paper we present a theory of two-dimensional "sheet" polymers. We investigate the static conformations as well as the dynamics of these objects. Some of our conclusions (mostly related to static conformations) have been summarized elsewhere.[2] Here we give a more detailed exposition, as well as some new results.

Recently there have been many studies of random surfaces.[3-8] However, in contrast to polymers, there is not a single universality class encompassing all types of surfaces.[8] Most studies have focused on random surfaces related to high-temperature plaquette expansions of lattice gauge theories.[3,4] In such models, surfaces of planar topology are built on a lattice (sometimes more complicated topologies are also used), and the statistical weight W attributed to a configuration depends only on the total surface area S. Since these surfaces are usually treated in a manner allowing the total surface area to vary, while the statistics is controlled by $W(S)$, the statistical problem is often called the "canonical ensemble." The resulting surfaces are highly ramified, and closely resemble branched polymers.[3,4,7] Here, on the other hand, we are interested in modeling sheets of covalently bonded atoms, or polymerized lipid surfaces, for which a natural starting point is to consider possible deformations of a *fixed* network of plaquettes,[5,6] or of particles placed at the sites of such a network. Since the number of plaquettes in such a surface does not vary, this statistical problem is frequently referred to as the "microcanonical ensemble." Such nomenclature is *very misleading* since it implies that they represent two different ("canonical" and "microcanonical") points of view for the same object. Actually, the two types of surfaces only share the same (planar) topology, but their thermodynamic behaviors belong to different universality classes. The most important property of the sheets of atoms considered here is their fixed internal connectivity[8] (e.g., a sixfold triangular network). To distinguish them from other types of surfaces they will be referred to as "tethered," or "fixed-connectivity" surfaces. If there are *mobile* disclinations (i.e., points of fivefold and sevenfold coordination in a triangular net, or threefold and fivefold coordination in a square net), then the internal structure of the surface will be "liquid"[9] and it may resemble more the canonical random plaquette surfaces.

Surfaces without mobile disclinations are "quasi-isometric," in the sense that the shortest path between any two sites typically traverses an identical number of bonds, regardless of configuration. It is interesting to note that the local Gaussian curvature of a *rigorously* isometric surface is unchanged by arbitrary bending and crumpling.[10] Here, the constraint of invariant local Gaussian curvature is imposed only approximately: For the discretized triangulated surfaces studied in this paper, the local Gaussian curvature can be approximated by the deviation of the coordination number from six;[11] sites of fivefold coordination will have on average a positive curvature, while sevenfold sites will be hyperbolic. In this paper we shall restrict our attention to six coordinated surfaces whose intrinsic Gaussian curvature is therefore constrained to be approximately zero everywhere. Only the *extrinsic* curvature fluctuates strongly in a quasi-isometric surface.

A simple example of fixed-connectivity surfaces is a collection of hard spheres tethered by strings of finite ex-

tension into a 2D triangular net, embedded in d-dimensional space. In the absence of self-avoiding restrictions, we find that at large distances the surface behaves elastically, due to entropic effects. The analogous result for polymers follows from simple random walk ideas.[1] For tethered surfaces, we demonstrate this important result in Sec. II via a real-space renormalization-group procedure, and by direct numerical Monte Carlo (MC) simulation. We show that in the absence of self-avoidance the radius of gyration R_G grows with the linear (uncrumpled) size of the surface L as $R_G^2 \sim \ln L$. Results of this section enable us to obtain a continuum description of tethered surfaces. In Sec. III we analyze self-avoiding surfaces and show that their radius of gyration increases as $R_G \sim L^\nu$.[12] We generalize the Flory argument for polymers[1] to obtain the estimate $\nu_F = 4/(d+2)$ for surfaces, a result which is in good agreement with our numerical simulations of the network embedded in three dimensions (3D). Since the mass (area) of the surface grows as L^2, the exponent ν is related to the fractal,[13] or Hausdorff, dimension by $d_f = 2/\nu$. The Flory-theory prediction is then $d_{f;F} = d/2 + 1$.

The nonlinear couplings generated by self-avoiding restrictions produce a complicated dynamic scaling behavior, discussed in Sec. IV. We make theoretical predictions for the case of Rouse dynamics that can be checked by our MC simulations. The inclusion of "back-flow" effects, and long-range interactions for surfaces in fluids leads to new hydrodynamic relaxations. Unlike polymers, where hydrodynamic and self-avoiding interactions both cease to be relevant above $d > 4$, surfaces have a range of dimensionalities ($d > 6$) where self-avoidance still dominates, but hydrodynamic interactions are unimportant. Our simulations are used to probe the nontrivial Rouse dynamics which remains when the hydrodynamic effects are excluded. Section V describes the results of a "table-top" experiment of actually crumpling sheets of foil. Even such a crude procedure leads to a nontrivial fractal dimension which, surprisingly, coincides with the Flory prediction. Finally, in Sec. VI we discuss the applicability of our results to various physical systems such as network glasses or polymeric surfaces. Various curious coincidences, and possible avenues for further research in this intriguing subject are explored.

II. PHANTOM SURFACES

We consider a system of particles connected to form a triangular 2D lattice, and embedded in d-dimensional space (the precise 2D lattice is not important, as long as the connections between its sites are fixed). Each particle is labeled by a 2D internal coordinate $\mathbf{x} = (x_1, x_2)$ with discrete x_1 and x_2 (in some orthogonal basis) denoting its place on the network. For our triangular lattice, it is convenient to choose two primitive vectors $\{\mathbf{a}^{(1)}; \mathbf{a}^{(2)}\}$ of equal length a, making an angle of 60°. The locations of the atoms in terms of the internal coordinates will be given by

$$\mathbf{x} = (m_1 + \tfrac{1}{2})\mathbf{a}^{(1)} + (m_2 + \tfrac{1}{2})\mathbf{a}^{(2)} , \qquad (2.1)$$

where m_i's are integers. (The reason for the shift of coordinates by $\tfrac{1}{2}$ will become apparent in Sec. IV.) The actual

location of the atom in the embedding space is described by the d-dimensional external coordinate $\mathbf{r}(x_1, x_2)$. The Hamiltonian with pairwise nearest-neighbor interactions is

$$\frac{\mathcal{H}}{k_B T} = \sum_{\langle \mathbf{x}, \mathbf{x}' \rangle} V[\,|\,\mathbf{r}(\mathbf{x}) - \mathbf{r}(\mathbf{x}')\,|\,] . \qquad (2.2)$$

Since the self-avoiding restrictions between distant parts of the surface are ignored at this stage, Eq. (2.2) describes a phantom network. The statistical mechanics associated with Eq. (2.2) can be solved exactly for a Gaussian potential $V(r) = (K_0/2)r^2$. For $|\mathbf{x} - \mathbf{x}'| \gg a$, the mean value of $|\mathbf{r}(\mathbf{x}) - \mathbf{r}(\mathbf{x}')|^2$, for example, is given by

$$\langle\,|\,\mathbf{r}(\mathbf{x}) - \mathbf{r}(\mathbf{x}')\,|^2\,\rangle = \frac{d}{\pi\sqrt{3}K_0}\ln(\,|\mathbf{x} - \mathbf{x}'|\,/a) . \qquad (2.3)$$

Gross and others[5] have studied a related model with an elastic energy associated with changes in the areas of elementary triangles. Since the correlations in the latter model also grow logarithmically the two models appear to be in the same universality class.

The radius of gyration can be defined, in analogy to polymers, by

$$R_G^2 \equiv \frac{1}{2S^2} \int d^2x \int d^2x' \langle\,|\,\mathbf{r}(\mathbf{x}) - \mathbf{r}(\mathbf{x}')\,|^2\,\rangle , \qquad (2.4)$$

where the integrals extend over a surface with area S. For a Gaussian phantom surface like that discussed above of linear size L, we have $R_G^2 \sim \ln L$, i.e., the squared radius of gyration scales with the system size in the same way as $\langle\,|\,\mathbf{r}(\mathbf{x}) - \mathbf{r}(\mathbf{x}')\,|^2\,\rangle$ evaluated with $\mathbf{x}$ and $\mathbf{x}'$ on opposite sides of the surface. This alternative measure is analogous to the end-to-end distance in a polymer.

Although the Gaussian potential is easily solvable, it is nevertheless useful to observe the following analogy with electrostatics: The procedure of calculation of $\langle\,|\,\mathbf{r}(\mathbf{x}) - \mathbf{r}(\mathbf{x}')\,|^2\,\rangle$ is formally identical with the calculation of the resistance $\mathcal{R}(\mathbf{x}, \mathbf{x}')$ between two points of a triangular resistor network,[14] built of elementary resistances $1/K_0$, and therefore $\langle\,|\,\mathbf{r}(\mathbf{x}) - \mathbf{r}(\mathbf{x}')\,|^2\,\rangle = d\mathcal{R}(\mathbf{x}, \mathbf{x}')$. In particular, the logarithmic divergence mimics the behavior of an electrostatic potential of a charge in 2D. Similarly, on length scales comparable to the lattice spacing a there are deviations from the logarithmic behavior, exactly in the same way the 2D electrostatic potential deviates from a logarithm on a discrete lattice.

The continuum limit of the Gaussian spring network is

$$\frac{\mathcal{H}}{k_B T} = \frac{K}{2} \int d^2x \, (\nabla \mathbf{r})^2 , \qquad (2.5)$$

where $(\nabla \mathbf{r})^2 \equiv (\partial \mathbf{r}/\partial x_1)^2 + (\partial \mathbf{r}/\partial x_2)^2$, and the continuum force constant K is related to the discrete force constant of the triangular lattice by $K = K_0\sqrt{3}$. Although it leads to an easily solved continuum limit, the discrete Gaussian potential differs significantly from any realistic two-body potential, and the large length-scale behavior for other potentials $V(r)$, is less obvious. For (linear) polymers the Markovian nature of the chain enables calculation of the long wavelength properties of arbitrary $V(r)$.[1] Because fixed-connectivity surfaces cannot be solved in a similar manner (even for the phantom networks), we must resort to more approximate techniques.

One such method is to construct an approximate renormalization group via the Migdal-Kadanoff bond-moving approximation for integrating out the intermediate particles.[15] We first "move" the interactions as shown in Fig. 1 to produce an isolated one-dimensional set of degrees of freedom. This approximate "bond-moving" step conserves the number of bonds in the original problem, and allows exact decimation of a subset of particles. Upon integrating out these one-dimensional degrees of freedom we obtain a new potential for a triangular lattice with lattice constant $b = 2$, namely

$$V'(\mid \mathbf{r}_1 - \mathbf{r}_2 \mid) = -\ln \left[\int d^d r_0 \exp[-2V(\mid \mathbf{r}_1 - \mathbf{r}_0 \mid)]$$

$$-2V(\mid \mathbf{r}_0 - \mathbf{r}_2 \mid)] \right]. \qquad (2.6)$$

The above procedure can be clearly repeated with any rescaling factor b. Since the decimation in Eq. (2.6) is a convolution of weight functions, the results can be more compactly written in terms of the Fourier-transformed weight function $\widetilde{W}(q) = \int d^d r \, e^{i\mathbf{q}\cdot\mathbf{r}} W(r)$, where $W(\mathbf{r}) \propto \exp[-V(\mathbf{r})]$. For a rescaling by factor b in the bond-moving step $W(r) \to W_{\text{int}}(r) = [W(r)]^b$, and in the decimation stage $\widetilde{W}'(q) = [\widetilde{W}_{\text{int}}(q)]^b$. Thus the Migdal-Kadanoff rescaling by factor b is obtained by raising the weight to the power of b in the real space, and then in the Fourier space. One advantage of this procedure is that it is exact on certain realizable "hierarchical" lattices.[16] Thus if we start with any positive normalizable initial weight W, it will remain positive and normalizable under subsequent renormalizations.

It can be verified analytically that any Gaussian potential is exactly invariant under this transformation [Eq. (2.6)], indicating a fixed line. We found numerically that a variety of potentials, including the "rigid rod" potential which forces the neighboring points to remain at a fixed distance, and the hard-sphere and -string potential, converge to Gaussians under renormalization. The latter potential represents behavior of a system of hard spheres (in our simulations they were of unit diameter) tethered into a triangular network by strings of maximal extent $\sqrt{3}$ [i.e., $V(r) = 0$ for $1 < r < \sqrt{3}$, and ∞ otherwise], embedded in three dimensions. Figure 2(a) depicts the results of Migdal-Kadanoff rescaling of such potential. The original weight function $W(r)$ limits the distance between neighboring atoms to a small interval between 1 and $\sqrt{3}$. However, already after the first rescaling we obtain a weight function which is closer to a Gaussian than to the original weight function. The number of iterations of the

transformation necessary to approach the Gaussian fixed potential defines a persistence length ξ for the surface. From Fig. 2(a) one sees that after three rescalings we obtain a result which is barely distinguishable from a Gaussian, and therefore $\xi \approx 8$. We can extract a renormalized spring constant K_R from the fixed-point weight function $W^*(r)$ via the definition

$$W^*(r) \equiv \exp(-\tfrac{1}{2}K_R r^2) . \qquad (2.7)$$

The renormalized spring constant provides a measure of the large distance entropy-generated elasticity. In this approximate rescaling procedure we get $K_R \approx 0.7$.

The successive iterations of a rigid rod potential are depicted in Fig. 2(b). This time the convergence is some-

(a)

(b)
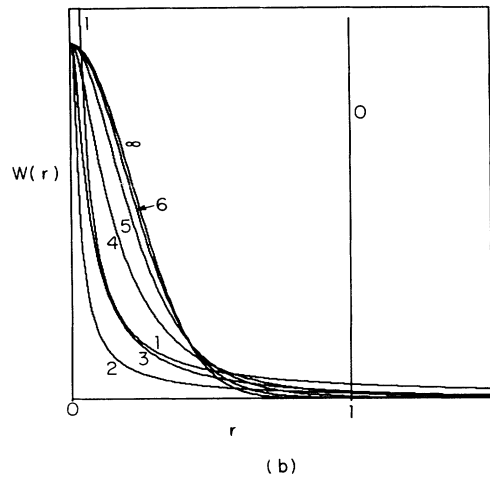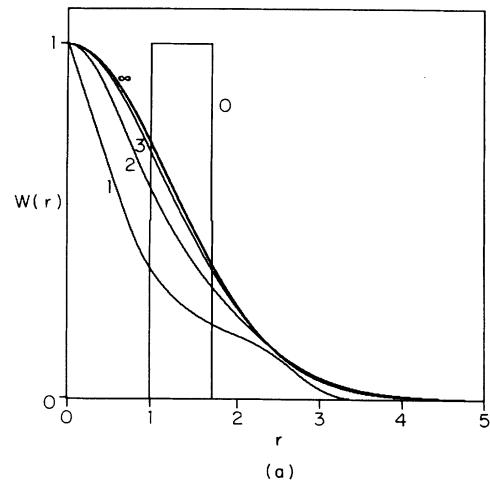
FIG. 2. Migdal-Kadanoff rescaling of the (a) hard-sphere and -tether and (b) rigid rod potentials. The curves show the dependence of the renormalized weight function $W(r)$ on the interparticle distance r. A constant is added to $V(r)$ to insure that $W(r)$ tends to unity at $r = 0$ after many iterations. The numbers near the curves indicate how many times the rescaling transformation has been applied. The label 0 corresponds to the original weight function; ∞ the limit to which the weight functions converge under rescaling. [The vertical line (0) in (b) represents a δ function.]
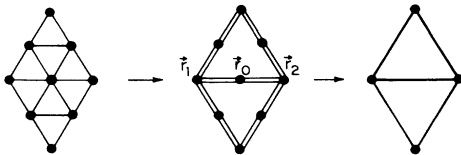

FIG. 1. Migdal-Kadanoff rescaling procedure for a triangular lattice: The approximate bond moving step, which produces isolated one-dimensional degrees of freedom, is followed by exact decimation.

what slower: After one rescaling, the original weight function $W(r) \sim \delta(r-1)$ produces a singular (but normalizable) weight function $W'(r) \sim 1/r$, for $r < 2$, and 0 otherwise. The following iterations produce results which start resembling a Gaussian. Finally after six iterations the result is already barely distinguishable from the asymptotic Gaussian shape.

Going beyond the approximate rescaling of the potential, the asymptotic Gaussian behavior was confirmed numerically by a MC simulation of the system. Our hard-sphere and -string model of the surface closely resembles the standard models used to simulate linear polymers.[17] Since our potentials do not introduce an energy scale into the problem, the results are independent of temperature, and the free energy is solely due to entropy effects. Such potentials may be expected to generate small persistence lengths, and thus reduce the crossover effects. Another advantage of this potential lies in the simplicity of MC procedure, since the statistical weights are either 1 or 0.

We sampled the configuration space using the "Brownian dynamics" method:[18] during a "MC time unit" we attempt to update the position of each atom by adding a vector of length s with randomly chosen direction to its current position. For a single isolated atom this corresponds to a Brownian motion with diffusion coefficient $D_0 = s^2/(2d)$. In the simulation each such attempted move is accepted only if the new position of the atom is allowed by the potentials. (We used $s = 0.2$, for which about half of the attempted moves are accepted in the case of self-avoiding surfaces, which will be discussed in Sec. III.) The procedure is a simplified version of the general Brownian dynamics algorithm. It satisfies the detailed balance conditions,[18] and therefore we may expect that after a sufficient time the surface approaches equilibrium. We perform the MC simulations for $L \times L$ parallelograms (here L measures the number of atoms) with free edges, cut out of a triangular lattice with L ranging from 2 to 16, as depicted in Fig. 3. The internal coordinates of the atoms are given by Eq. (2.1) with $m_i = 0, 1, \ldots, l = L - 1$.

Because the MC procedure generates a highly correlated sequence of configurations, the actual sampling of configurations (for the results reported in this and next sections) was made only every $\tau_0 = L^2/s^2$ time steps, and the total length of each simulation was $100\tau_0$. It will be shown in Sec. IV, that the time τ_0 is approximately equal to the Rouse relaxation time $\tau_R(L)$ of the phantom surface, during which the free surface "forgets" its initial configuration. Thus, for phantom surfaces we sampled completely independent configurations. The computation time per τ_0 increases as L^4 ($\tau_0 \sim L^2$, and during each MC time unit we try to update the positions of L^2 atoms). The largest ($L = 16$) surface required 8 h of CPU (central processing unit) time on Apollo DN460 computer.

The average R_G^2 of such a surface is depicted in Fig. 4 as a function of its linear size L. The initial slope of the graph is somewhat large, because the hard-sphere repulsion between the nearest neighbors still has a noticeable effect on the overall behavior. Eventually, the curve approaches a simple logarithmic behavior as in the Gaussian model. To facilitate the comparison of the tethered surface with a Gaussian surface, we performed an exact cal-
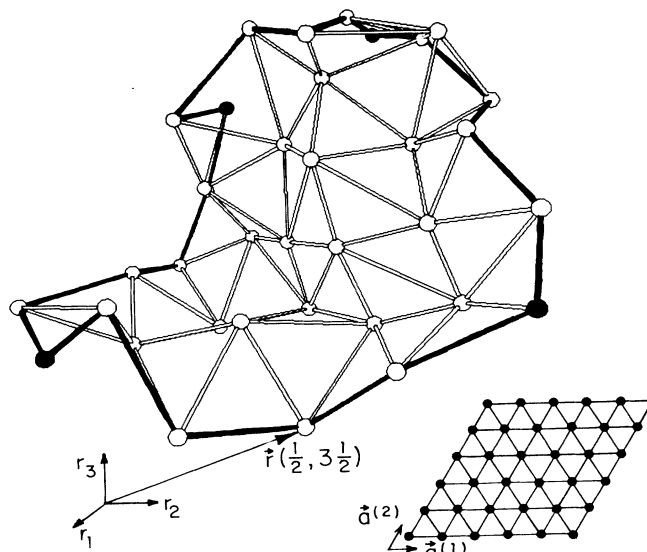

FIG. 3. Triangular tethered surface with $L = 6$. The picture in the lower right corner depicts the topology (connectivity) of the system. Positions of the atoms on the surface are determined by two-dimensional internal coordinates $\mathbf{x}$ [see Eq. (2.1)]. The actual positions of the atoms as shown in the main figure are the three-dimensional external coordinates $\mathbf{r}(\mathbf{x})$. (Bonds located at the boundary of the parallelogram and corner atoms are shown in black.)

culation of $R_G^{(0)}$, the radius of gyration of a discrete Gaussian surface with spring constant $K_0 = 1$, which has the same connectivity and shape as our surface. Both surfaces have similar lattice and finite size effects. The ratio

$$K_{\text{eff}} \equiv [R_G^{(0)}(L)/R_G(L)]^2 \qquad (2.8)$$

should then smoothly approach K_R as L tends to infinity. As shown in Fig. 4, this ratio does indeed approach a constant for large L, with effective coupling $K_R \approx 0.63$, remarkably close to the $K_R \approx 0.7$ obtained from the approx-
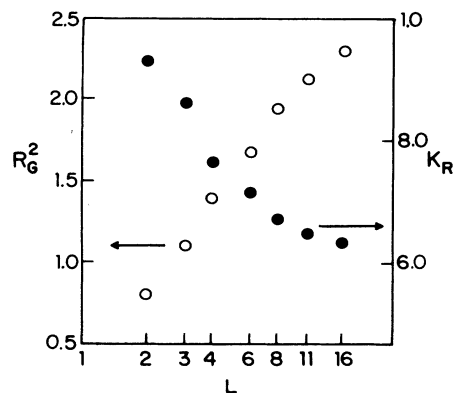

FIG. 4. Semilogarithmic plot of R_G^2 of the free surface ($\bigcirc$), and of K_R($\bullet$) versus L.

imate Migdal-Kadanoff rescaling. The persistence length is again about 8.

Higher-order interactions, such as those embodied in bending energies,[19] complicate both the rescaling calculation and numerical simulations. On the basis of universality, however, we expect that these factors simply introduce a new (possibly temperature dependent) persistence length and modify the force constant. Provided the persistence length remains finite, we do not expect such modifications to alter the appearance of entropy-generated harmonic forces at large distances in phantom fixed-connectivity surfaces.

III. SELF-AVOIDING SURFACES OF FIXED CONNECTIVITY

Our next step is to consider more tangible surfaces, with self-avoidance. We first attempt a continuum description of the problem, by generalizing the Edwards model[20] for polymers. The partition function Z is obtained by summing over all configurations of the surface $r(x)$ (the 2D internal coordinate x is now continuous), with a Hamiltonian, similar to (2.5), to which a term accounting for the excluded volume interaction has been added:

$$Z = \int \mathscr{D}r \exp\left[-\frac{K}{2} \int d^2x (\nabla r)^2 \right.$$
$$\left. -\frac{v}{2} \int d^2x \int d^2x'\, \delta^d(r(x)-r(x')) \right],$$
$$(3.1)$$

where the interaction v measures the "excluded volume" as in the case of polymers.[1] Hamiltonians of this kind can, in principle, be treated by renormalization group methods.[21] Here, however, we limit ourselves to the investigation of more elementary properties of the surfaces. First we carry out a perturbation expansion[22] in v about the phantom surface. As shown in the Appendix, the mean value of the squared distance between two points x and x', separated by L along the internal coordinates is, to leading order in v,

$$\langle |r(x)-r(x')|^2 \rangle$$
$$= \frac{d\ln L}{\pi K}\left[1 + \frac{\pi^2 v}{8}\left[\frac{K}{2} \right]^{d/2} \frac{L'^4}{(\ln L')^{1+d/2}} \right]. \quad (3.2)$$

Up to an unimportant coefficient the cutoff length L' is equal to L. The distance increases with v as expected, but the coefficient of v diverges for large $L' \sim L$. By contrast, in a similar expansion for polymers the coefficient decays with L above $d=4$,[1,22] allowing a systematic expansion in $\epsilon = 4-d$. Equation (3.2) suggests that self-avoidance can only be neglected for elastic surfaces when $d = \infty$, in agreement with the observation of Gross[5] that the fractal dimension of the noninteracting surface is infinite.

Divergent perturbation theory implies a nontrivial scaling that can by studied by a Flory-type approximation.[1] Consider a surface of internal size L, occupying a region of size R_G in d-dimensional space. According to Flory we may approximate the free energy to

$\mathscr{F} \approx \frac{1}{2}KR_G^2 + \frac{1}{2}vL^4/R_G^d$. The first term represents the elastic (entropic) energy of a phantom surface (up to a term $\ln L$, which has been replaced by a constant), while the second term is a mean-field estimate of the repulsive interaction energy $[(\text{volume})\times(\text{density})^2 \approx L^4/R_G^d]$. By minimizing $\mathscr{F}$ we find $R_G \sim (v/K)^{1/(d+2)}L^{\nu_F}$, with

$$\nu_F = 4/(d+2), \quad (3.3)$$

or $d_{f;F} = d/2 + 1$. (For a related calculation see Ref. 23.) Somewhat more formally we can determine ν_F from (3.1) by requiring,[21] that the rescaling factors of the internal coordinate x and the external coordinate r would be related in such a way that the ratio between the two terms in the integrand of (3.1) will remain unchanged under the rescaling. In any case, we expect the exponent ν to be bounded from below by $2/d$ (maximally compact surface), and from above by 1 (maximally stretched surface).

Despite its numerous deficiencies,[1] Flory-type theory produces remarkably good estimates of ν for linear polymers. Note, that in the case of surfaces (as in the case of polymers) it produces correct results in the lower ($d=2$, where $\nu=1$) and the upper ($d=\infty$, where $\nu=0$) critical dimensions. However, considering the large range between the critical dimensions compared to 1 and 4 in the case of linear polymers, we may wonder about the effectiveness of such an interpolation.

To test these predictions, the MC simulations were repeated for the tethered sphere surfaces described earlier but with self-avoiding restrictions (the centers of any two spheres cannot come closer than their diameter). The maximal string extension of $\sqrt{3}$ now ensures complete impenetrability of the surface. The equilibration of self-avoiding surfaces requires significantly longer times than the corresponding phantom surfaces. We started from a configuration in which all the atoms were in one plane, equilibrated the surface for $100\tau_0$, and performed various measurements during the next $100\tau_0$ ($150\tau_0$ for $L=11$), at every time interval τ_0. As will be shown in Sec. IV, the Rouse relaxation time $\tau_R(L)$ now scales like $L^{3.6}$. Since $\tau_0 \sim L^2$, the number of statistically independent configurations decreased with increasing L. While for $L=4$ all 100 configurations were independent, for $L=8$ we had only few such configurations, and for $L=11$ (the largest surface used) the total simulation time was equal to $\tau_R(L)$. Since the number of operations per MC time unit (for small surfaces) increases as L^4 (L^2 atoms are moved, and each attempt requires L^2 excluded volume checks with other atoms), the total simulation time per $\tau_R(L)$ increases as $L^{7.6}$. (For sufficiently large surfaces a more efficient algorithm, not requiring L^2 excluded volume checks, can be used. Thus, eventually the time will increase "only" as $L^{5.6}$. However, our surfaces are not yet sufficiently large.) The total CPU time per τ_R ($L=11$) on the Apollo DN460 computer was 140 h. Thus as significant additional increase of surface sizes is beyond our present capabilities.

A typical configuration generated by the simulation is plotted in Fig. 5(a). The particles in this perspective drawing have the correct ratio of the radius relative to the maximum possible separation of their centers. In Fig. 5(b), we show the same configuration, with the particles
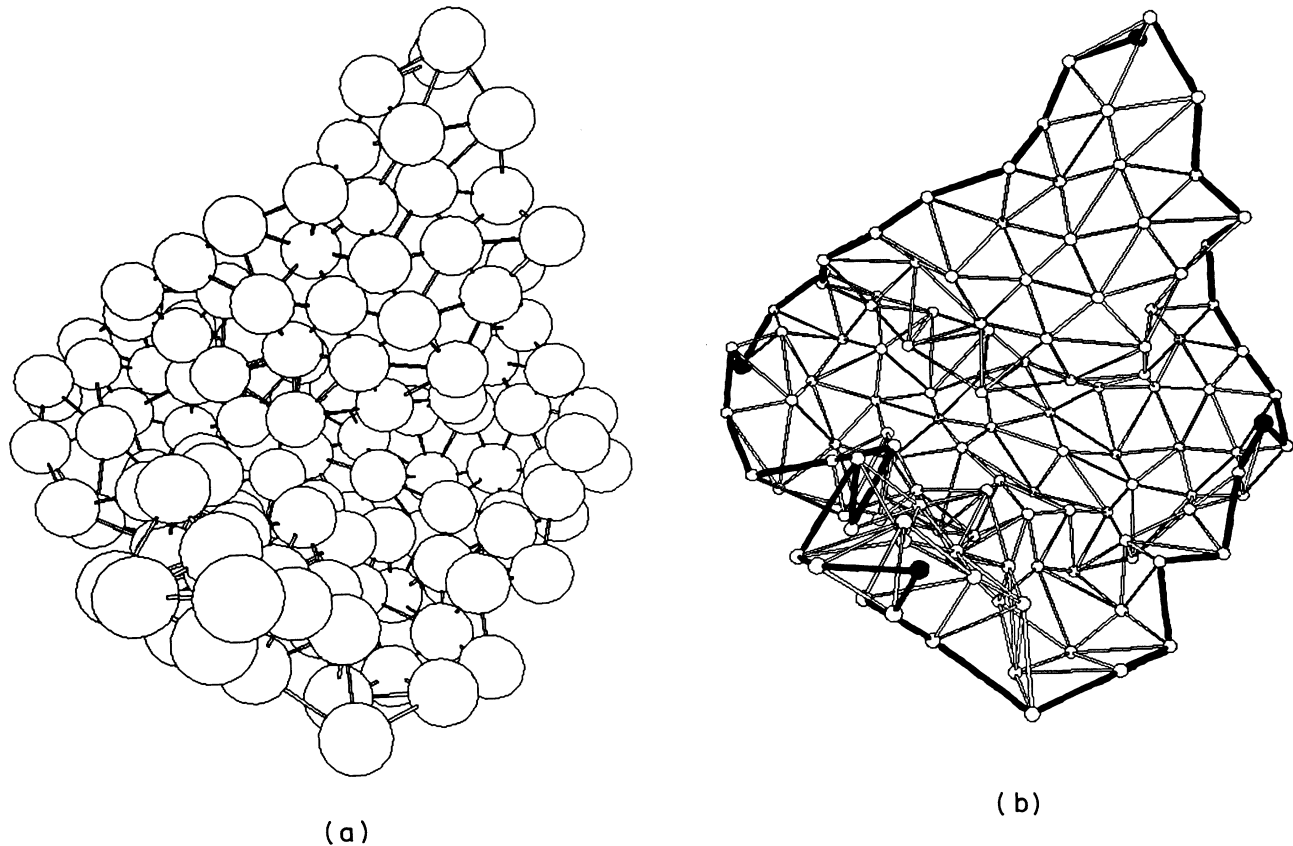
(a)

(b)

FIG. 5. (a) Shape of the self-avoiding surface for $L = 11$. Sphere sizes indicate the range of the repulsive potential. (b) "Skeleton" of the same surface: For clarity, the sizes of the atoms were taken to be $\frac{1}{5}$ of the actual range of the hard-core potential. Bonds indicate the nearest-neighbor atoms between which the string potential acts. Bonds located at the boundary of the parallelogram and the corner atoms are shown in black.

now drawn $\frac{1}{5}$ of their actual size to better illustrate the crumplings involved. To study the scaling properties of these surfaces, the mean-squared radius of gyration (Fig. 6) has been calculated as a function of L. We find a nice power law dependence with $v = 0.83 \pm 0.03$. To check the validity and the accuracy of the procedure, we repeated the MC calculation for a single chain of atoms (i.e., a polymer). The results of that simulation are also shown in Fig. 6. For the polymer we obtain $v = 0.64$, which overestimates the known value of v, but is reasonable in view of the short chains considered.

The surface appearing in Fig. 5 is very nonspherical. We obtained a quantitative estimate of departure from sphericity, by calculating the mean values of the ratios of the principal moments of inertia (eigenvalues of the tensor of inertia) for the surfaces. Those ratios are depicted in Fig. 7. They appear to be almost independent of the size of the surface. The ratio between the smallest and the largest principal moments ≈ 0.16, and the ratio between the intermediate and the largest moments ≈ 0.45. (Analogous ratios for phantom surfaces slowly increase with L and reach the respective values 0.47 and 0.63 for $L = 16$,
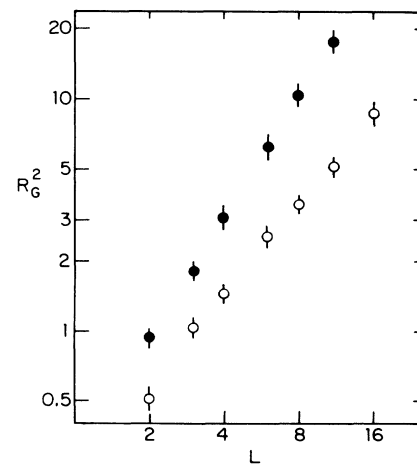

FIG. 6. Logarithmic plot of R_G^2 of the self-avoiding surface (●) versus L. Error bars indicate the standard deviation of the R_G^2. Analogous results for a linear self-avoiding chain are also shown (○).
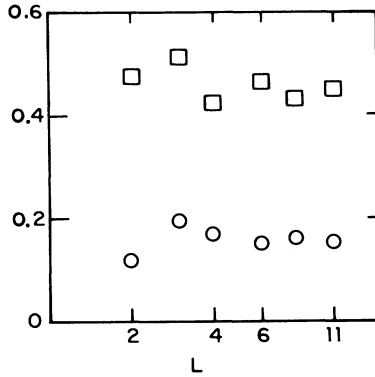
FIG. 7. Semilogarithmic plot of the mean ratios between the principal moments of inertia (O, smallest/largest; □, intermediate/largest) versus the size L of the surface.
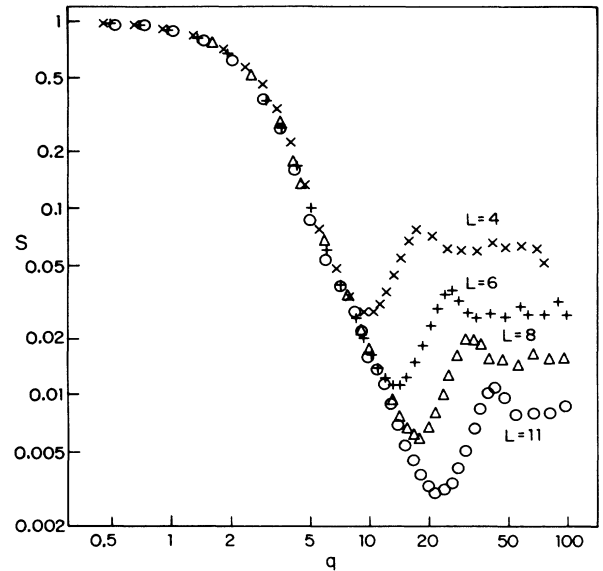

FIG. 8. Logarithmic plot of the structure factor S as a function of $q \equiv kL^\nu$, with $\nu=0.83$. (Some overlapping data points have been omitted for clarity.)

i.e., the phantom surfaces are considerably more spherical. This is different from polymers in which self-avoidance does not appreciably change the ratios of principal moments of inertia.[24] For linear polymers, those ratios are in fact universal numbers.[24] For surfaces we may expect that those ratios do not depend on the small scale details of the surface (such as a particular choice of a lattice, or potential), but they may depend on the overall shape of the surface in internal space.

The main source of the possible errors in the simulation of such small surfaces are not the statistical errors, but rather "systematic errors" which appear since we are not in the asymptotic regime. Thus it is useful to have two distinct ways to estimate ν, e.g., directly from the two-point (density-density) correlation function and from the "mass versus radius of gyration" curve. Differences in the exponents obtained by those methods provide an estimate of the "systematic error." We examined the Fourier transform of the two-point correlation function (or structure factor)

$$S(\mathbf{k},L) \equiv \frac{1}{L^4} \sum_{\mathbf{x},\mathbf{x}'} \left\langle e^{i\mathbf{k}\cdot[\mathbf{r}(\mathbf{x})-\mathbf{r}(\mathbf{x}')]} \right\rangle \ . \tag{3.4}$$

In analogy with polymer systems,[18] we expect that the structure factor satisfies the scaling form $S(\mathbf{k},L)=S(kR_G)=S(kL^\nu)$.[18] Indeed, as indicated in Fig. 8, the measured $S(k,L)$ for different values of L all collapse into a single function, when plotted against the scaling variable $q=kL^\nu$ with $\nu=0.83\pm0.03$. This "data collapse test" is essentially identical to the direct measurement of ν from Fig. 6. The good data collapse even on short length scales means that $\xi\approx1$, i.e., the bare parameters of our Hamiltonian are close to their asymptotic values. The structure factors in Fig. 8 have the following characteristic features: For small $q(k<R_G^{-1})$ all curves have identical parabolic behavior, since $S(k)=1-\frac{1}{3}k^2R_G^2+\cdots=1-\mathrm{const}\times q^2+\cdots$; for $k\sim1$ we see the typical short length-scale structure (oscillations) of a hard sphere gas; for $k\gg1$ the oscillations decay and $S(k)=1/L^2$. To satisfy the latter condition for large L,

we must require $S(q)\sim q^{-2/\nu}$ for intermediate q, and indeed this behavior is obtained in Fig. 8. From the slope in Fig. 8 we estimate $\nu=0.77\pm0.03$, providing us with an alternative estimate of the critical exponent. Our overall estimate is a value of the critical exponent is

$$\nu=0.80\pm0.05 \ , \tag{3.5}$$

or fractal dimension $d_f=2/\nu=2.5\pm0.15$, where the error bars indicate our subjective assessment of the possible systematic errors. This result is in good agreement with the value of $\nu_F=\frac{4}{5}$, thus confirming the accuracy of the Flory approximation and the physics embodied in Eq. (3.1).

IV. DYNAMICS OF TETHERED SURFACES

Most of the dynamical aspects of linear polymers in a solvent are fairly well understood.[1] In this section we present the generalization of some of these results to the dynamics of surfaces.

The simplest possible model of polymer dynamics has been introduced by Rouse.[25] In this model the (usually important[26]) long-range hydrodynamic interactions between different parts of the polymer are ignored. Each part of the surface is assumed to move under the influence of the surface forces (surface stretching due to near-neighbor and excluded volume forces due to distant neighbors), and a random force representing thermal noise. The dynamics is assumed to be purely diffusive, since the contribution of the inertial terms can be neglected for sufficiently long times. While such a model may not be realistic in most experimental situations, it nevertheless is important for the following reasons. (a) In some circumstances, such as motion of a polymer through a solid matrix[27] (via vacancy diffusion), this may actually be the

correct description of the process. (b) The Brownian dynamics method used in the MC simulation actually corresponds to Rouse dynamics, and it is important to know various time dependent quantities: e.g., to obtain meaningful static results we must know the "waiting times" between two statistically independent configurations. (c) We also notice that the hydrodynamic interactions are relevant only in the case[28] when $d_f > d - 2$. In this case the hydrodynamic flow does not penetrate the object, and it behaves as a solid sphere. For $d_f < d - 2$ the hydrodynamic flow penetrates the object, meaning that the distortion of a flow by a single monomer is limited (not sufficiently long ranged), and therefore those interactions can be disregarded. Assuming $d_f = d/2 + 1$, we find that the hydrodynamic interactions become irrelevant for $d > 6$. Note that this is quite different from the case of regular polymers: For a linear polymer the hydrodynamic interactions are irrelevant for $d > 4$, i.e., at the same dimensions where the excluded volume interactions can be neglected, while in the case of surfaces at $d > 6$, we cannot neglect the excluded volume.

We start our analysis by considering the simplest case of Rouse dynamics of a phantom surface of linear dimensions $L \times L$, in the continuum limit. Motion of the surface is described by a Langevin equation

$$\frac{1}{\mu}\frac{\partial \mathbf{r}(\mathbf{x},t)}{\partial t} = K'\nabla^2 \mathbf{r}(\mathbf{x},t) + \boldsymbol{\zeta}(\mathbf{x},t) , \qquad (4.1)$$

where μ is the mobility of a unit surface area, which is related to the diffusion constant D by $D = \mu k_B T$, and $\nabla^2 \mathbf{r} \equiv \partial^2 \mathbf{r}/\partial x_1^2 + \partial^2 \mathbf{r}/\partial x_2^2$. The first term on the right-hand side of Eq. (4.1) represents the force exerted on a given point by the neighboring points, connected to it by Gaussian springs, with spring constants $K' = K k_B T$. The second term represents the random (Brownian) force, whose autocorrelation function is

$$\langle \zeta_\alpha(\mathbf{x},t)\zeta_\beta(\mathbf{x}',t') \rangle = \frac{2k_B T}{\mu}\delta^2(\mathbf{x}-\mathbf{x}')\delta(t-t')\delta_{\alpha\beta} , \qquad (4.2)$$

where $\langle \ \rangle$ denotes the average over the noise ensemble. It can be checked that the Fokker-Planck equation associated with (4.1) relaxes to the probability distribution associated with Hamiltonian (2.5). As in the case of a linear polymer,[25,26,29] Eq. (4.1) separates in Rouse coordinates (or normal modes) which, in the case of the surface, are the 2D cosine transforms in the *internal* coordinates $\mathbf{x}$ of the surface of the *external* position vector $\mathbf{r}$:

$$\mathbf{u}(\mathbf{Q},t) \equiv \frac{1}{L^2}\int \prod_{i=1}^{2}(dx_i \cos Q_i x_i)\mathbf{r}(\mathbf{x},t) , \qquad (4.3)$$

where $\mathbf{Q} = (\pi/L)(n_1,n_2)$ $(n_i = 0,1,2,3,\ldots)$ is the 2D wave vector. We prefer the particular form (4.3) to more standard Fourier transforms (suitable for periodic boundary conditions), since, as will be shown in the discussion of discrete surfaces, the pure modes (4.3) satisfy more physical boundary conditions. Applying the cosine transform to Eq. (4.1) we obtain

$$\frac{1}{\mu}\frac{\partial \mathbf{u}(\mathbf{Q},t)}{\partial t} = -K'Q^2\mathbf{u}(\mathbf{Q},t) + \boldsymbol{\zeta}(\mathbf{Q},t) , \qquad (4.4)$$

where $\boldsymbol{\zeta}(\mathbf{Q},t)$ are the cosine transforms of the original

noise functions satisfying

$$\langle \zeta_\alpha(\mathbf{Q},t)\zeta_\beta(\mathbf{Q}',t') \rangle = \frac{2k_B T}{\mu L^2}\delta_{\mathbf{Q}\mathbf{Q}'}\delta(t-t')\delta_{\alpha\beta}f_{\mathbf{Q}} , \qquad (4.5)$$

where $f_{\mathbf{Q}}$ is $\frac{1}{2}$ to the power of number of nonzero components of the vector $\mathbf{Q}$. By solving the Eq. (4.4) we can find the autocorrelation function of the Rouse modes:

$$\langle u_\alpha(\mathbf{Q},t)u_\beta(\mathbf{Q}',t') \rangle = \delta_{\alpha\beta}\delta_{\mathbf{Q}\mathbf{Q}'}\frac{k_B T f_{\mathbf{Q}}}{K'Q^2 L^2}e^{-K'Q^2\mu|t-t'|} . \qquad (4.6)$$

This solution is only valid for $\mathbf{Q}\neq 0$. The $\mathbf{Q} = 0$ Rouse mode is exactly the coordinate of the center of mass of the surface, which diffuses as a simple particle, with mobility μ/L^2. The slowest nonzero internal relaxation mode of the surface has $Q^2 = \pi^2/L^2$; it follows from (4.6) that its relaxation time is

$$\tau_R(L) = \frac{L^2}{\pi^2 K'\mu} = \frac{L^2}{\pi^2 KD} . \qquad (4.7)$$

In our MC simulation we used a triangular lattice with effective force constant $K_0 \approx 0.63$, corresponding to a continuum coupling $K \approx \sqrt{3}K_0 \approx 1$. Recall that the diffusion constant of a single atom is $s^2/6$, where $s = 0.2$ is the distance an atom can be moved in one MC time unit. This diffusion constant has to be divided by $\sqrt{3}/2$ (surface area per atom) to obtain the continuum diffusion constant D. Substituting these values into (4.7), we find $\tau_R \approx L^2/s^2 = \tau_0$, i.e., the time unit used to determine the length of our MC simulation was of the order of the Rouse relaxation time of our model. (The nonsquare shape of our sample modifies this estimate by a factor of order unity.) The general expression for the relaxation times of the Rouse modes of a *rectangular* surface of size $L_1 \times L_2$ is given by

$$\tau_R(n_1,n_2) = \left\{ \pi^2 K'\mu \left[\left[\frac{n_1}{L_1}\right]^2 + \left[\frac{n_2}{L_2}\right]^2 \right] \right\}^{-1} . \qquad (4.8)$$

It is worth noting that the L dependence of the slowest internal relaxation time of the phantom surface coincides (up to a logarithmic correction) with the time during which the center of mass of the surface diffuses a distance equal to its radius of gyration. This relation for phantom surfaces, also follows from the general scaling considerations.[1] It is believed to be valid in general, both for polymers with self-avoiding restriction, and in the cases where the dynamics is governed by hydrodynamic forces.

Introduction of a discrete surface (as opposed to the continuum model treated above) does not modify our results in any significant way: Consider, for example, a square lattice with lattice constant a, in which the internal coordinates of atoms are given by $a(m_1 + \frac{1}{2}, m_2 + \frac{1}{2})$ $(m_i = 0,1,\ldots,l = L-1)$. The appropriate wave vectors will be $\mathbf{Q} = (\pi/La)(n_1,n_2)$ $(n_i = 0,1,\ldots,l)$, and the Rouse modes will be given by a discrete version of Eq. (4.3):

$$\mathbf{u}(\mathbf{Q},t)=\frac{1}{L^2 a^2}\sum_{m_1,m_2=0}^{l}\left[\prod_{i=1}^{2}\cos\left[\frac{\pi n_i(m_i+\frac{1}{2})}{L}\right]\right]$$

$$\times\mathbf{r}(m_1,m_2)\ . \qquad (4.9)$$

The only change in the continuum equations will be the replacement of Q^2 in Eq. (4.4) by $(2/a^2)(2-\cos Q_1 a-\cos Q_2 a)$. Clearly, this modification does not change the results for $Q\ll 1/a$. In principle, Eq. (4.1) must be supplemented with the boundary conditions, although these are not very important for the modes with $Q\gg 1/(La)$. The natural choice, corresponding to the physical situation, is that of free boundaries. The Rouse modes defined in Eqs. (4.3) and (4.9) satisfy these boundary conditions: The periodicity of the Rouse modes is such that the boundary atoms satisfy relations of the type $\mathbf{r}(m_1,m_2=l)=\mathbf{r}(m_1,m_2=l+1)$, etc. (The shift of the coordinates by $\frac{1}{2}$ was made to assure this property.) Thus, we may think of our surface as a part of a larger surface, on which the positions of the atoms are chosen in such a manner that a boundary atom of the original surface is located at the same point as its nearest neighbor from outside the surface. Therefore no force is applied at the boundary atom by the atoms outside the boundary, and the solution corresponds to free boundaries.

In the case of a parallelogram-shaped surface cut out of a triangular lattice, which is used in our simulations, it is convenient to choose the basis vectors $\{\mathbf{a}^{(1)};\mathbf{a}^{(2)}\}$, which were defined in Sec. II. Although now we have a nonrectangular coordinate system, we still may use the definition (4.9), where m_i's will be interpreted as coordinates of atoms expressed in $\{\mathbf{a}^{(1)};\mathbf{a}^{(2)}\}$ basis vectors, while $\pi n_i/La$ will be the coordinate of the wave vector in a reciprocal coordinate system $\{\mathbf{b}^{(1)};\mathbf{b}^{(2)}\}$ in which $(\mathbf{b}^{(1)})^2=(\mathbf{b}^{(2)})^2$ $=-2\mathbf{b}^{(1)}\cdot\mathbf{b}^{(2)}=4/(3a^2)$. In this basis the squared length of a vector is $Q^2=(4\pi^2/3L^2a^2)(n_1^2+n_2^2-n_1n_2)$. Unfortunately, the Rouse modes of the triangular lattice defined in this manner no longer satisfy the free boundary conditions. (The argument applied to the square lattice is no longer valid since the boundary atoms have two nearest neighbors from outside the boundary.) We will nevertheless retain the notation as the most convenient nomenclature for Rouse modes on a triangular lattice.

The self-avoiding restrictions considerably modify the relaxation times of the tethered surface. We cannot solve the problem as explicitly as it has been done for the phantom surface. (However, problems of this type can be treated within the renormalization group framework.[21]) We shall, however, present a simple scaling argument, adapted from a discussion of the analogous problem in polymer physics.[1] It can be shown by a direct calculation[30] that the force constant of a polymer whose equilibrium radius of gyration is R_G is given by $K_{tot}\approx k_BT/R_G^2$. We shall assume a similar result for self-avoiding surfaces. Since the mobility of the entire surface in rouse dynamics is simply $\mu_{tot}=\mu/L^2$, we can treat the entire system as a simple (overdamped) oscillator satisfying $(1/\mu_{tot})(\partial\mathbf{r}/\partial t)=-K_{tot}\mathbf{r}$. This leads to a characteristic relaxation time

$$\tau_R=1/(\mu_{tot}K_{tot})\approx L^2R_G^2/(\mu k_BT)\sim L^{2+2\nu}$$

$$\sim R_G^{2+2/\nu}\ . \qquad (4.10)$$

As in the case of the phantom surface, the relaxation time is equal to the time required for the surface to diffuse its radius of gyration. In polymer physics it is customary to introduce the dynamical exponent z, describing the relaxation processes, defined by $\tau_R\sim R_G^z$. Thus in our case $z=2+2/\nu$. An analogous expression for (linear) polymers would yield $z=2+1/\nu$. Notice that the coefficient of $1/\nu$ indicates the dimensionality of the polymer (1 for a linear polymer, 2 for the surface). We observe that while the behavior of a self-avoiding (linear) polymer barely differs from the behavior of a Gaussian chain ($\tau_R\sim L^{2.2}$ instead of L^2), in the case of surfaces we expect a major difference ($\tau_R\sim L^{3.6}$ instead of L^2). Figure 9 depicts the evolution of an $L=11$ surface during $150\tau_0\approx\tau_R$ ($L=11$), as viewed from a fixed direction. During that time the surface both rotates an appreciable angle, and "unfolds." Comparing the large length-scale features at the "snapshots" taken every $50\tau_0$, we observe strong correlations. The short length-scale features appear to be completely independent, since their correlation times are shorter that $50\tau_0$.

A different relaxation mechanism, namely reptation,[31] occurs for polymers in the presence of fixed obstacles, and is easily generalizable to surfaces. Consider a surface trying to diffuse out of a confining cage, consisting of two frozen boundaries built along its two sides. The cage restricts the surface particles to longitudinal motions (i.e., along the walls of the cage). The fact that the surface is crumpled in the space becomes irrelevant, and we may think of it as moving in a 2D plane, and the "escape from the cage" is equivalent to diffusing a distance L. The time it takes for a surface, with diffusion constant proportional to $1/L^2$, to move distance L is proportional to L^4. We might expect that the relaxation process of a free (not confined) surface will be considerably faster and hence L^4 provides us with an upper bound. The exponent $z\nu$ has thus a lower bound of 2 coming from the relaxation of a phantom surface, and an upper bound of 4 corresponding to reptation from a confining cage. The value $z\nu=2+2\nu=3.6$ given in Eq. (4.10) indeed satisfies these bounds, and is close to its upper limit.

We checked the validity of Eq. (4.10) in our MC simulation. It is important to realize that the above derivation of the dependence of τ_R on the radius of gyration can be performed even in the case of a completely rigid object, and the resulting time simply indicates how long it takes for an object of a given size to rotate, say, by 90°, or to diffuse its own R_G, even though the internal degrees of freedom are completely "frozen." The real check of the scaling argument does not come from the measurement of the L dependence of the slowest relaxation times, but from the fact that relation (4.10) holds also on length scales smaller than the size of the surface. We therefore examined relaxation of the Rouse modes in our surfaces and checked whether the relation $\tau_R\sim Q^{-3.6}$ holds for all modes (and not just the slowest ones). During our MC procedure we calculated the Rouse modes at each instance and studied the autocorrelation functions
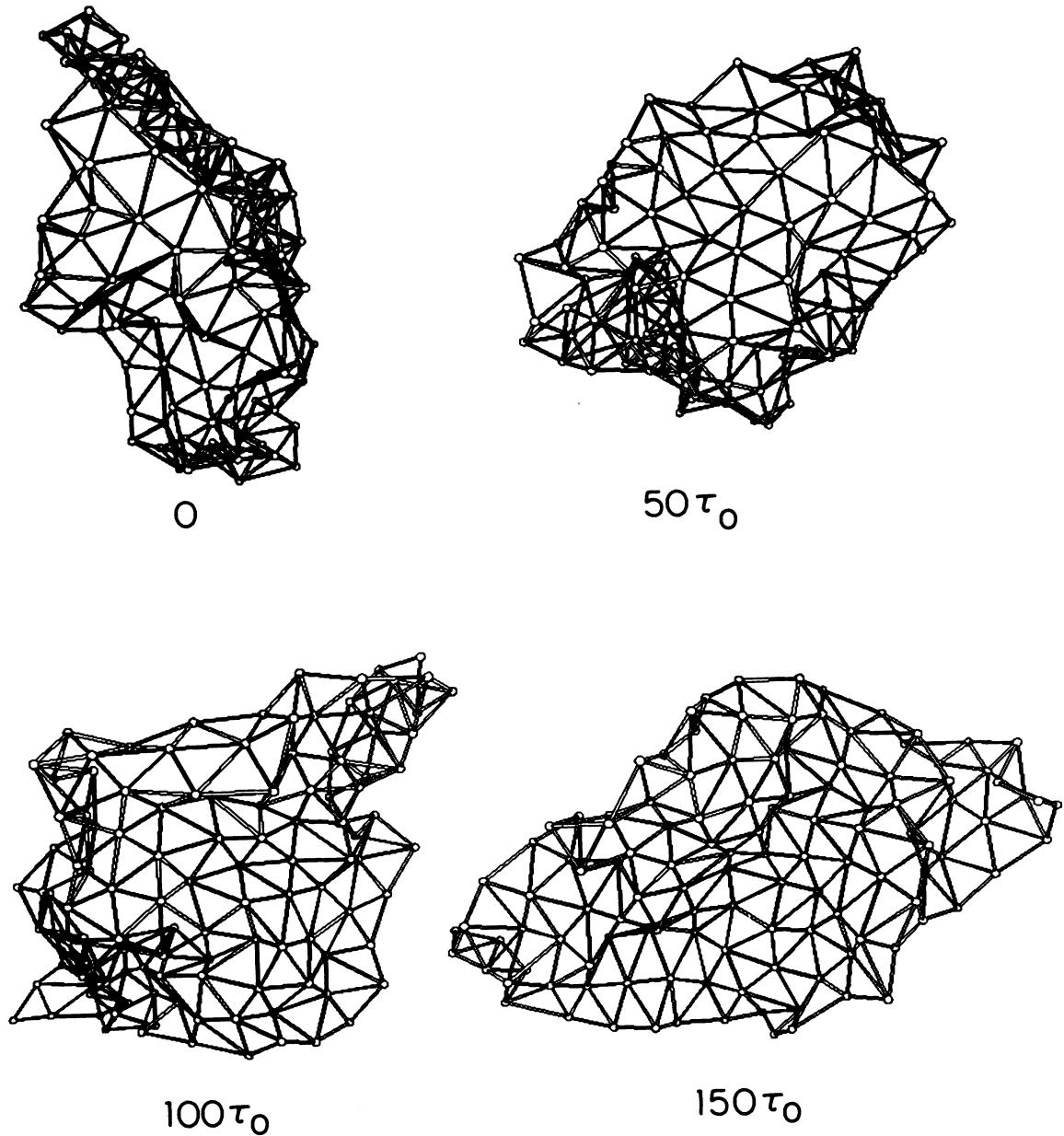
O

$50\tau_0$

$100\tau_0$

$150\tau_0$

FIG. 9. Time evolution of $L = 11$ surface during one $\tau_R \approx 150\tau_0$.

$C_Q(t - t') \equiv \langle \mathbf{u}(\mathbf{Q},t)\cdot\mathbf{u}(\mathbf{Q},t')\rangle$. Of course, we can no longer expect $C_Q(t)$ to be a simple exponential, as in phantom surfaces, because these are no longer the eigenmodes of the self-avoiding surface. However, we may expect to be able to extract a reasonably well defined time for each $\mathbf{Q}$. Figure 10 depicts the autocorrelation function of several Rouse modes in the $L = 8$ surface. The averaging was performed over the time span of $100\tau_0$.

Figure 10(a) shows the three slowest modes of the surface. (Note, that the [1,0], [0,1], and [1,1] modes correspond to the same value of $|\mathbf{Q}|$.) We immediately see the strong effect of the finite size (boundary), on the relax-

ation times. The decay of correlations in the [1,1] mode is by an order of magnitude faster, than in the other two. The shape of the surface affects the correlations in different ways: [1,0] and [0,1] wave vectors are perpendicular to the boundaries of the parallelogram, while the [1,1] wave vector is directed along the long diagonal. The effective width of the surface in the direction perpendicular to the [1,1] wave vector is smaller and therefore the correlations decay faster. The second observation is that the autocorrelation functions of [1,0] and [0,1] modes do not coincide for $t > 75\,000$, despite the fact that (by symmetry) they should be identical. This is a direct result of the
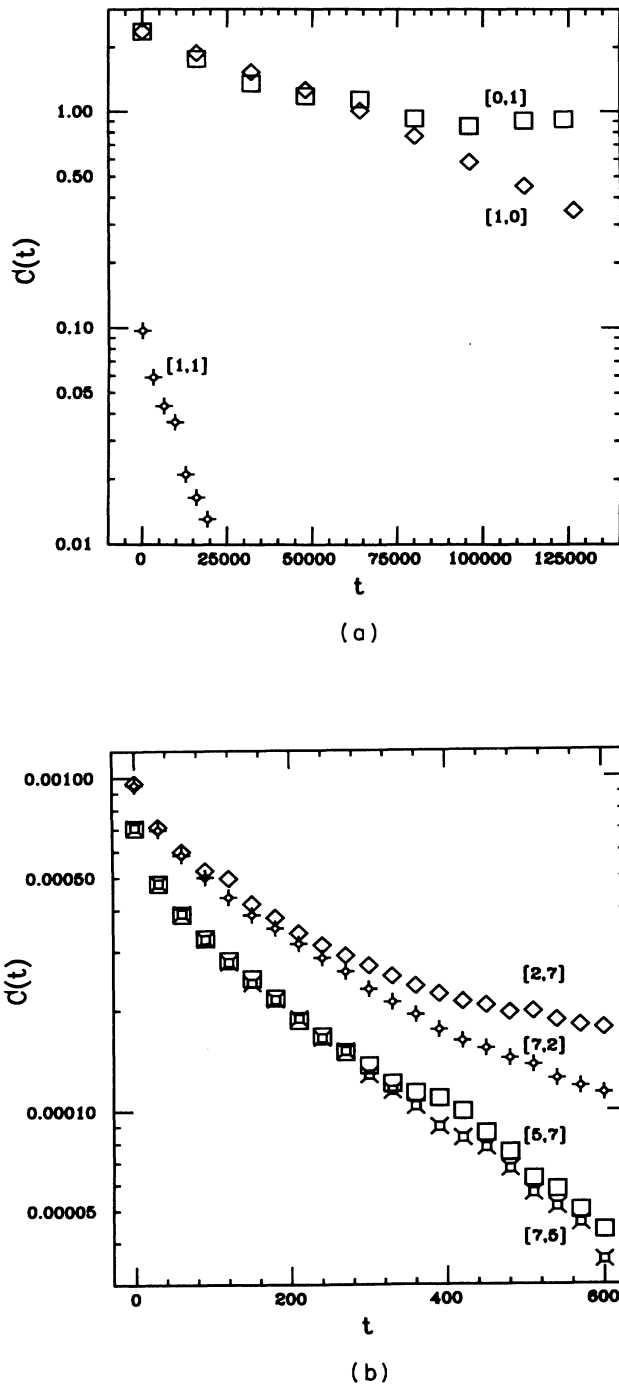
(a)

(b)

FIG. 10. Semilogarithmic plots of the autocorrelation functions of Rouse modes of $L = 8$ surface. Numbers $[n_1, n_2]$ indicate the particular mode selected. (a) Slowest mode of the surface. All three modes have the same $|Q|$. The differences between the equivalent modes [1,0] and [0,1] demonstrate the noise (finite simulation time) effect. Significantly different behavior of [1,1] mode indicates the strong effect of the boundaries. (b) Intermediate modes of the surface. All four modes have the same $|Q|$. Noise and boundary effects are much smaller than in (a).

finite simulation time: Values of $C(t)$ have been obtained by averaging over $100\tau_0 = 160\,000$. Since the relaxation time of the mode is about 80 000 (the exact value depends on the definition) we actually sampled only about two independent configurations. We therefore may expect that the size of the "statistical noise" will be almost of the order of $C(0)$. Indeed the departure of the two graphs appears when the value of $C(t)$ decays to $\frac{1}{2}$ of its initial value. The example of Fig. 1(a) provides us with an estimate of the region where the results of the statistical average can be trusted. The results depicted in Fig. 10(b), show that most of the problems of small-Q modes disappear, when we go to the range of intermediate Q's. First we see that the $C(t)$ curves of equivalent (from the point of view of boundary conditions) Rouse modes coincide over most of the decay, since the sampling times are now much longer than typical correlation times. In addition, we see that both pairs of modes have a very similar behavior. Indeed all four modes have the same $|Q|$, indicating that for sufficiently large Q's the behavior depends only on the absolute size of Q, and not on its orientation relative to the boundaries of the sample.

The shapes of the $C(t)$ curves can be reasonably fitted by a sum of two exponentials with a ratio of decay times approximately 2:1. Since the curves are rather noisy, we did not attempt to use this method, and, instead, defined the characteristic decay time $\tau_R(Q)$ as a time during which $C(t)$ decayed to $1/e$ of its initial value. For fast (large Q) modes we obtained 10% accuracy. For the slowest modes of the $L = 8$ and 11 surfaces, however, we could only estimate the time, and the errors may be as large as 50%. This, however, did not influence significantly our conclusions, since the data points range over 4 orders of magnitude in time. Results for relaxation times of all Rouse modes of all surface sizes are depicted in Fig. 11. The true scaling regime is very small even for the
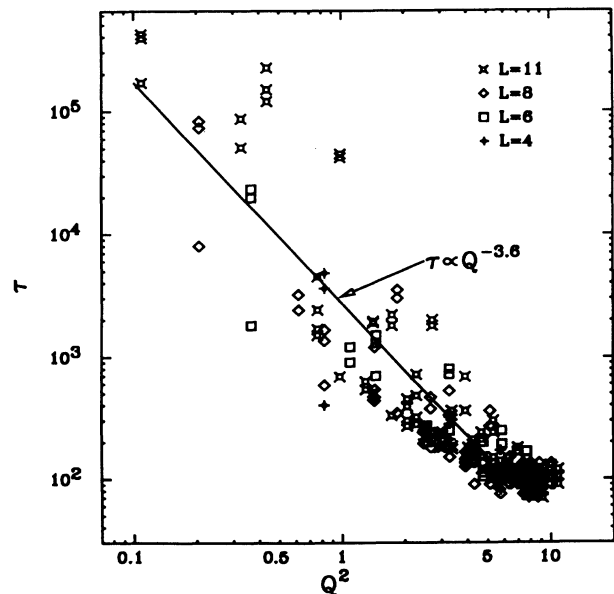

FIG. 11. Logarithmic plot of the relaxation times of all Rouse modes of surfaces of all sizes versus Q^2 (in lattice units). The straight line indicates the behavior which was predicted from the scaling considerations.

largest $(L=11)$ surface, since for small Q's we have strong boundary effects, while for large Q's the discreteness of the surface is being felt. Thus, we cannot expect to obtain a very good estimate of the exponent. The straight line in Fig. 11 is just a guide to the eye, indicating that the exponent $zv=3.6$ is consistent with the data. From the large scatter we can only estimate the possible error to be ± 0.5.

A more quantitative estimate of the exponent zv can be obtained only from considerably larger surfaces, which for the reasons explained in Sec. III, cannot be simulated at the present time. In principle, it is also possible to calculate the exponent z from the observation of the behavior of the surface in the real space. Just as in polymeric systems,[32] it can be shown that at time scales shorter than the largest relaxation time of the surface, a typical particle displacement $\langle |\mathbf{r}(\mathbf{x},t)-\mathbf{r}(\mathbf{x},0)|^2\rangle$ grows algebraically as $t^{2/z}$, while beyond that time it crosses over to a regular diffusion (identical with diffusion of the center of mass of the surface). We did not attempt to analyze our data in this manner, since it is essentially equivalent to the method we use, but produces "smoothening" of the data, hiding the actual large scatter of the points, as revealed in Fig. 11.

The exponent z depends on the dynamics imposed on the system. If hydrodynamical interactions are taken into account, we will get a very different result. We still may use the arguments which lead us to Eq. (4.10), except that the mobility of the surface will now be determined by hydrodynamic interactions: For $d_f > d-2$ (i.e., when $d<6$) the surface is not transparent to the hydrodynamic flow and behaves as a solid sphere of radius R_G. In this case $\mu_{tot} \sim R_G^{2-d}$, and consequently $\tau_{hydro}(L) \sim R_G^d \sim L^{dv}$ $\sim L^{2d/d_f}$, or $z=d$. Note, that when $d_f=d-2$ (or $d\approx 6$), this result coincides with τ_R of Eq. (4.10), which was calculated neglecting the hydrodynamic effects. Beyond that point (for larger d's) the behavior of the surface is given by the Rouse dynamics.

V. CRUMPLED SURFACES

We stated in Sec. III, that the lower bound on the value of v is $2/d$, which corresponds to a compact packing. Surfaces which actually achieve this bound are far from trivial, since the numerous constraints of a fixed-connectivity surface restrict the possibilities of folding. The reader is invited to try to fold an $L\times L$ surface of thickness h into a cube of linear size $L^{2/3}h^{1/3}$. If the surface can be stretched only by a certain fixed percentage (a quasi-isometric surface) then most of the simple foldings will not allow compactification of the surface for sufficiently large L. If the surface is elastic, then we will find that simple foldings require energy which increases faster than the surface area. Nevertheless, we know of at least one folding which allows compactifying the surface.[33]

Considering the difficulties associated with finding an "intelligent" compactification procedure, it should not come as a surprise that randomly crumpled surfaces are not compact. We carried out a "table-top experiment" by actually randomly (and irreversibly) crumpling sheets of foil. We started with square pieces of different linear size

L, and proceeded to crumple them into approximately spherical balls. The measured diameters of the balls are depicted in Fig. 12 as functions of the uncrumpled linear size L. As this figure indicates, the diameter scales as L^v with $v\approx 0.8$, or $d_f\approx 2.5$,[34] which coincides with the Flory exponent for the statistics of tethered surfaces in equilibrium.

Although the crumpling procedure of this experiment is rather ill defined and appears quite haphazard, we would like to point out that the "random crumpling" process is very strongly constrained by the surface connectivity and the choices of a particular crumpling procedure are quite limited. Although we did not specify the force with which the final crumpled surfaces have been compressed, the compression process is very nonlinear and beyond a certain compression the diameter of the surface does not change appreciably. (The amplitude of the power law in Fig. 12 will decrease slightly with increasing force, but the exponent is probably unchanged.) Clearly, the physics of the crumpling process differs significantly from the thermal equilibration of surfaces. Nevertheless, the identity of v's in both processes, may be more than a pure coincidence, since the random crumpling "explores the configuration space" in a way which somewhat resembles the behavior of equilibrated tethered surfaces. To fully understand this result we need a better understanding of the energetic and topological roles played by the creases on the surface, and their intersection points.

VI. DISCUSSION

There are a number of extensions and possible applications of the results presented in this paper.

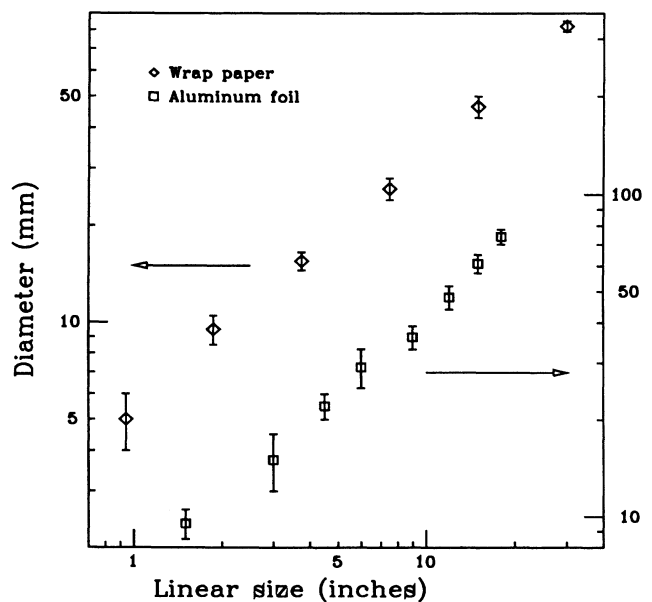(1) Our results for the statics naturally imply that a

FIG. 12. Logarithmic plot of the external diameter of crumpled surfaces versus their original (uncrumpled) linear size. The error bars indicate the variability of the diameter (departure from sphericity).

straight line of length l drawn on the fully extended surface will occupy a volume of size $l^{4/5}$, while a self-avoiding walk on the extended surface, occupies a region of size $l^{3/4}$. Upon crumpling into d dimensions, the walk will extend over a size $(l^{3/4})^\nu \sim l^{3/(d+2)}$, which, remarkably, coincides with the Flory prediction for polymers in d dimensions $(d \leq 4)$. This is a more general property of Flory-type theories: If we have a D-dimensional (self-avoiding) object in d-dimensional space then Flory theory predicts[35]

$$\nu(D,d)=(D+2)/(d+2) . \tag{6.1}$$

If we have three different dimensionalities, d_1, d_2, and d_3, then

$$\nu(d_1,d_2)\nu(d_2,d_3)=\nu(d_1,d_3) . \tag{6.2}$$

Another application follows from regarding a 3D self-avoiding walk, with Flory exponent $\nu(1,3)=\frac{3}{5}$, as inscribed on a three dimensional "surface" embedded in four dimensions. Crumpling of the 3D surface into four dimensions is controlled by the Flory exponent $\nu(3,4)=\frac{5}{6}$, so the exponent of the 3D self-avoiding walk crumpled in four dimensions is the mean-field result $\nu=\frac{3}{5} \cdot \frac{5}{6}=\frac{1}{2}$. It would be interesting to know whether the "transitivity" of Eq. (6.2) is valid beyond the Flory approximation. In any case, it is clear that a 3D self-avoiding walk created by a crumpling of a 2D surface with a 2D self-avoiding walk is not identical with a regular 3D walk. This can be clearly seen if the walk on the 2D surface forms a closed loop. When "crumpled into the third dimension" it will generate a loop *without knots*. Thus the ensembles are not identical, but it would be interesting to find whether such constructions could be used to investigate effects of topological constraints.

(2) For a strip of width w and length l, we may observe a crossover from self-avoiding polymers to tethered surfaces. For $w < l$ we expect to get $R_G \sim w^{\nu_2 - \nu_1} l^{\nu_1}$, where ν_1 and ν_2 are the respective exponents for linear polymers and surfaces. Within the Flory theory this result has (for $d \leq 4$) the form $R_G \sim (wl^3)^{1/(d+2)}$.

(3) Laboratory examples of surfaces discussed in this paper are provided by 2D polymer networks (2D gels[1]). Some lipid molecules polymerize into sheets with multiple crosslinks upon exposure to ultraviolet radiation.[36] A *bilayer* of this kind with the polar head groups facing out would presumably enter an aqueous solvent and provide another example of the surfaces studied here. Spherical vehicle bilayers have already been polymerized in this way.[37] Light-scattering experiments from dilute solutions would yield direct information on the exponent ν and the dynamical fluctuations of individual surfaces. In dense solutions, surfaces do not interpenetrate and (unlike regular polymers) are far from ideal. The situation is somewhat like a dense polymer melt in *two* dimensions. Our results may also be relevant to 2D network glasses, such as As_2S_3 or B_2O_3.[38] Just above the glass transition, the liquid presumably consists of many crumpled sheets of covalently bonded molecules. Understanding the statistical mechanics of an isolated sheet is a first step towards dealing with this problem. The large increase in volume (about 30%) of molten B_2O_3 relative to its crystalline form may be related to the swelling of an isolated surface

discussed here.[39] Of course, a covalently bonded sheet of B_2O_3 need not have the simple planar topology assumed in this paper.

(4) Charged polymers, or polyelectrolytes, are known to have drastically different behavior than the ordinary polymers, when the Debye screening length exceeds the radius of gyration.[40] In less than four dimensions electrolytic polymers are fully stretched (i.e., $\nu=1$). As has been pointed out in Ref. 40, in the case of a charged polymer the renormalization group provides an *exact* value of the exponent ν. Application of that technique to the tethered surfaces shows that for $d \leq 6$ charged surfaces are completely stretched, while for $d > 6$, we have[41]

$$\nu=4/(d-2) , \tag{6.3}$$

which differs from the Flory estimate $\nu=3/d$ for $d \geq 3$.

(5) It is interesting to note that the fractal dimension $d_f=2.5$ of a self-avoiding surface is the same as the set on which strong velocity fluctuations are concentrated in models of intermittent, fully-developed turbulence.[42,43] The fact that these fluctuations do not occupy all of space (i.e., $d_f < 3$) leads to deviations from the famous Kolmogorov spectrum $E(k) \sim k^{-5/3}$, and to nontrivial behavior of higher-order velocity cumulants.[43] Our results for self-avoiding surfaces suggest that it may be possible to model turbulence by crumpled sheets of vorticity[44] in an otherwise quiescent fluid.

We hope that the results and speculations presented in this paper will lead to further investigations into the physics of tethered surfaces.

ACKNOWLEDGMENTS

APPENDIX: PERTURBATION THEORY FOR RANDOM SURFACES

In this Appendix, we show how to calculate surface correlations perturbatively in the excluded volume parameter v. Instead of the partition function (3.1), consider the generating function

$$C_\mathbf{p}(x_1,x_2)=\langle e^{i\mathbf{p}\cdot[\mathbf{r}(x_1)-\mathbf{r}(x_2)]} \rangle , \tag{A1}$$
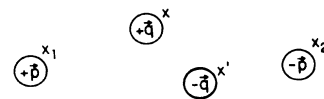

FIG. 13. Geometric meaning of the integration variables in the Appendix.

where the average is taken with respect to the Hamiltonian associated with (3.1), namely

$$\frac{\mathcal{H}}{k_B T} = \frac{K}{2} \int d^2x \, |\nabla \mathbf{r}(x)|^2 + \frac{v}{2} \int d^2x \int d^2x' \, \delta^d(\mathbf{r}(x) - \mathbf{r}(x')) \, . \quad \text{(A2)}$$

Here we leave implicit the vector character of the two-dimensional variables such as x_1, x_2, x, and x' in order to distinguish these quantities from the d-dimensional *external* vectors such as $\mathbf{p}$, $\mathbf{r}(x_1)$, and $\mathbf{r}(x_2)$.

To the lowest order in v, we can write

$$C_{\mathbf{p}}(x_1, x_2) = \langle e^{i\mathbf{p}\cdot[\mathbf{r}(x_1) - \mathbf{r}(x_2)]} \rangle_0 - \frac{v}{2} \int d^2x \int d^2x' [\, \langle \delta^d(\mathbf{r}(x) - \mathbf{r}(x')) e^{i\mathbf{p}\cdot[\mathbf{r}(x_1) - \mathbf{r}(x_2)]} \rangle_0$$
$$- \langle \delta^d(\mathbf{r}(x) - \mathbf{r}(x')) \rangle_0 \langle e^{i\mathbf{p}\cdot[\mathbf{r}(x_1) - \mathbf{r}(x_2)]} \rangle_0] + O(v^2) \, , \quad \text{(A3)}$$

where $\langle \bullet \rangle_0$ means an average with respect to the unperturbed Hamiltonian,

$$\langle \bullet \rangle_0 = \frac{\int \mathcal{D}\mathbf{r}(x) \bullet \exp\left[-\frac{1}{2}K \int d^2x \, |\nabla \mathbf{r}|^2 \right]}{\int \mathcal{D}\mathbf{r}(x) \exp\left[-\frac{1}{2}K \int d^2x \, |\nabla \mathbf{r}|^2 \right]} \, . \quad \text{(A4)}$$

In what follows we shall often have to evaluate averages of the form

$$\left\langle \exp\left[i \sum_\alpha \mathbf{p}_\alpha \cdot \mathbf{r}(x_\alpha) \right] \right\rangle_0 \, ,$$

with $\sum_\alpha \mathbf{p}_\alpha = 0$, for which it can be shown straightforwardly using (A4) that

$$\left\langle \exp\left[i \sum_\alpha \mathbf{p}_\alpha \cdot \mathbf{r}(x_\alpha) \right] \right\rangle_0 = \exp\left[\frac{1}{K} \sum_{\alpha < \beta} \mathbf{p}_\alpha \cdot \mathbf{p}_\beta G(x_\alpha - x_\beta) \right] \, , \quad \text{(A5)}$$

where $G(x)$ is a Green's function in the internal space satisfying

$$\nabla^2 G(x) = \delta(x) \, . \quad \text{(A6)}$$

For large x we have

$$G(x) = \frac{1}{2\pi} \ln|x| \, . \quad \text{(A7)}$$

We are now in the position to evaluate the different averages in (A3). Using an integral representation of the δ function, we have, for example,

$$\langle \delta^d(\mathbf{r}(x) - \mathbf{r}(x')) \rangle = \int \frac{d^dq}{(2\pi)^d} \langle e^{i\mathbf{q}\cdot[\mathbf{r}(x) - \mathbf{r}(x')]} \rangle_0$$
$$= \int \frac{d^dq}{(2\pi)^d} \exp\left[-\frac{q^2}{K} G(x - x') \right] \, , \quad \text{(A8)}$$

and

$$\langle e^{i\mathbf{p}\cdot[\mathbf{r}(x_1) - \mathbf{r}(x_2)]} \delta(\mathbf{r}(x) - \mathbf{r}(x')) \rangle_0$$
$$= \int \frac{d^dq}{(2\pi)^d} \langle e^{i\mathbf{p}\cdot[\mathbf{r}(x_1) - \mathbf{r}(x_2)] + i\mathbf{q}\cdot[\mathbf{r}(x) - \mathbf{r}(x')]} \rangle_0$$
$$= \int \frac{d^dq}{(2\pi)^d} \exp\left[-\frac{p^2}{K} G(x_1 - x_2) - \frac{q^2}{K} G(x - x') \right.$$
$$\left. + \frac{\mathbf{p}\cdot\mathbf{q}}{K} A(x_1, x_2; x, x') \right] \, , \quad \text{(A9)}$$

where the function $A(x_1, x_2; x, x')$ appearing in (A9) is given by

$$A(x_1, x_2; x, x') = G(x_1 - x) - G(x_1 - x')$$
$$- G(x_2 - x) + G(x_2 - x') \, . \quad \text{(A10)}$$

Combining the terms in (A3) together, we have

$$C_{\mathbf{p}}(x_1, x_2) = \exp\left[-\frac{p^2}{K} G(x_1 - x_2) \right]$$
$$\times \left\{ 1 - \frac{v}{2} \int d^2x \int d^2x' \int \frac{d^dq}{(2\pi)^d} \exp\left[-\frac{q^2}{K} G(x - x') \right] \left[\exp\left[\frac{\mathbf{p}\cdot\mathbf{q}}{K} A(x_1, x_2; x, x') \right] - 1 \right] + O(v^2) \right\} \, . \quad \text{(A11)}$$

The algebraic expressions above have a simple interpretation in terms of the statistical mechanics of vector charges interacting with logarithmic potential in two dimensions. As summarized in Fig. 13, for example, Eq. (A9) can be regarded as probability of a complexion of charges with fixed charges $\pm\mathbf{p}$ at x_1 and x_2 and variable charges $\pm\mathbf{q}$ at x and x'. This analogy is useful, because one can now adapt techniques developed for vector Coulomb gas models of two-dimensional melting[45] to the statistical mechanics of random surfaces. Although the final results are different, similar approximations can be made in both problems.

We now focus our attention on the second moment of $C_{\mathbf{p}}(x_1, x_2)$ and calculate $\langle |\mathbf{r}(x_1) - \mathbf{r}(x_2)|^2 \rangle$. Upon expanding both sides of (A11) in $\mathbf{p}$, and equating terms of order p^2, we obtain

$$\langle \, |\mathbf{r}(x_1)-\mathbf{r}(x_2)|^2 \rangle = \frac{2d}{K} G(x_1-x_2)$$

$$+ \frac{v}{2K^2} \int \frac{d^d q}{(2\pi)^d} q^2 \int d^2 x \int d^2 x' \exp\left[-\frac{q^2}{K} G(x-x')\right] [A(x_1,x_2;x,x')]^2 \tag{A12}$$

We assume that x_1 and x_2 are widely separated, and that the dominant contribution to the integral in (A12) comes from situations where x and x' are close together. The function $A(x_1,x_2;x,x')$ can be simplified by eliminating x and x' in favor of center-of-mass and relative coordinates

$$X = \tfrac{1}{2}(x+x') \, ,$$
$$y = x - x' \, , \tag{A13}$$

and expanding in y. To lowest order in y we have

$$A(x_1,x_2;x,x') = (y \cdot \nabla_X)[G(x_1-X) - G(x_2-X)] \, , \tag{A14}$$

and the integrals over x and x' in (A12) become

$$\int d^2 x \int d^2 x' \exp\left[-\frac{q^2}{K} G(x-x')\right] [A(x_1,x_2;x,x')]^2$$

$$= \int d^2 y \exp\left[-\frac{q^2}{K} G(y)\right] \int d^2 X \{(y \cdot \nabla_X)[G(x_1-X)-G(x_2-X)]\}^2 \, . \tag{A15}$$

This expression simplifies further upon carrying out an angular average over y, doing the X integration by parts and using

$$\nabla_X^2 [G(x_1-X) - G(x_2-X)] = \delta(x_1-X) - \delta(x_2-X) \, . \tag{A16}$$

Upon substituting in Eq. (A12), we obtain

$$\langle \, |\mathbf{r}(x_1)-\mathbf{r}(x_2)|^2 \rangle = \frac{2d}{K} G(x_1-x_2) \left[1 + \frac{\pi v}{2dK} \int_\alpha^{L'} d\,|y| \; |y|^3 \int \frac{d^d q}{(2\pi)^d} q^2 \exp\left[-\frac{q^2}{K} G(y)\right]\right] \, . \tag{A17}$$

The integral over y runs from a minimum internal distance a across which surfaces can interact to a maximum internal distance L' which is comparable to the system size if x_1 and x_2 are at the edges of the surface. Because the integral is strongly divergent at large distances the precise relationship between L and L' depends on the shape of the surface.

We can now easily complete the calculation. Carrying out the integrals over q we have

$$\int_\alpha^{L'} d\,|y| \; |y|^3 \int \frac{d^d q}{(2\pi)^d} q^2 \exp\left[-\frac{q^2}{K} C(y)\right]$$

$$= \frac{d}{2^{d+1}\pi^{d/2}} (2\pi K)^{1+d/2}$$

$$\times \int_\alpha^{L'} d\,|y| \; |y|^3 \frac{1}{[\ln|y|]^{1+d/2}} \, . \tag{A18}$$

The remaining integral over y is badly divergent, and dominated by the upper cutoff L'. Taking the separation $|x_1-x_2|$ to be the system size L, our final result is

$$\langle \, |\mathbf{r}(x_1)-\mathbf{r}(x_2)|^2 \rangle$$

$$= \frac{d \ln|x_1-x_2|}{\pi K}$$

$$\times \left[1 + \frac{\pi^2 v}{8}\left(\frac{K}{2}\right)^{d/2} \frac{L'^4}{(\ln L')^{1+d/2}}\right] \, , \tag{A19}$$

which agrees with Eq. (3.2). Note that there is an additional power of $\ln L'$ in the denominator of the second term in Eq. (A19) multiplying $(\ln L')^{d/2}$ which is expected from naive dimensional analysis.

[1]P. G. de Gennes, *Scaling Concepts in Polymer Physics* (Cornell University Press, Ithaca, New York, 1979).

[2]Y. Kantor, M. Kardar, and D. R. Nelson, Phys. Rev. Lett. **57**, 791 (1986).

[3]G. Parisi, Phys. Lett. **81B**, 357 (1979); J.-M. Drouffe, G. Parisi,

and N. Sourlas, Nucl. Phys. **B161**, 397 (1979).

[4]For a review, see J. Fröhlich, in *Applications of Field Theory to Statistical Mechanics*, Vol. 216 of *Lecture Notes in Physics*, edited by L. Garido (Springer, Berlin, 1985).

[5]A. Billoire, D. J. Gross, and E. Marinari, Phys. Lett. **139B**, 75

(1984); D. J. Gross, *ibid.* **139B**, 187 (1984).

[6]B. Duplantier, Phys. Lett. **141B**, 239 (1984).

[7]T. Eguchi and H. Kawai, Phys. Lett. **114B**, 247 (1982); T. Sterling and J. Greensite, *ibid.* **121B**, 345 (1983); H. Kawai and Y. Okamoto, *ibid.* **130B**, 415 (1983); B. Durhuus, J. Fröhlich, and T. Jonsson, Nucl. Phys. **B225**, 185 (1983); B. Berg and A. Billoire, Phys. Lett. **139B**, 297 (1984); A. Maritan and A. Stella, Phys. Rev. Lett. **53**, 123 (1984); S. Redner, J. Phys. A **18**, L723 (1985); U. Glaus, Phys. Rev. Lett. **56**, 1996 (1986).

[8]M. E. Cates, Phys. Lett. **161B**, 363 (1985).

[9]D. R. Nelson, Phys. Rev. B **26**, 269 (1982), and references therein.

[10]D. Hilbert and S. Cohn-Vossen, *Geometry and the Imagination* (Chelsea, New York, 1952), Sec. 29.

[11]See, e.g., D. R. Nelson, in *Topological Order in Condensed Matter*, edited by F. Yonezawa and T. Ninomiya (Springer, Berlin, 1983).

[12]In "canonical ensemble" surfaces, exponent ν defines the relation between R_G and *area* ($R_G \sim S^\nu$), since their *linear size L* is not well defined. For the fixed-connectivity surfaces we naturally extend the polymer notation and relate ν to L. Thus, our definition of ν is twice that of Refs. 4 and 7.

[13]B. B. Mandelbrot, *Fractals: Form Chance and Dimension* (Freeman, San Francisco, 1977); *The Fractal Geometry of Nature* (Freeman, San Francisco, 1982).

[14]The equivalence of the two problems follows from observation that the functional integral representation of resistance [see, e.g., M. J. Stephen, Phys. Rev. B **17**, 4444 (1978)] coincides (up to a prefactor d) with the statistical mechanical definition of $\langle |\mathbf{r}(\mathbf{x}) - \mathbf{r}(\mathbf{x}')|^2 \rangle$. This equivalence holds for *any* Gaussian network.

[15]L. P. Kadanoff, Ann. Phys. (N.Y.) **100**, 359 (1976). The particular procedure used here is similar to one used for *XY* models by A. N. Berker and D. R. Nelson, Phys. Rev. B **19**, 2488 (1979).

[16]A. N. Berker and S. Ostlund, J. Phys. C **12**, 4961 (1979); M. Kaufman and R. B. Griffiths, Phys. Rev. B **24**, 496 (1981).

[17]A. Baumgärtner, in *Applications of the Monte Carlo Method in Statistical Physics*, edited by K. Binder (Springer, Berlin, 1984), p. 145 and references therein.

[18]D. Ceperley, M. H. Kalos, and J. L. Lebowitz, Phys. Rev. Lett. **41**, 313 (1978); and Macromol. **14**, 1472 (1981).

[19]W. Helfrich, Z. Naturforsch. **28C**, 693 (1973); F. Brochard and J. F. Lennon, J. Phys. (Paris) **36**, 1035 (1975); F. Brochard, P. G. de Gennes, and P. Pfeuty, *ibid.* **37**, 1099 (1976); P. G. de Gennes and C. Taupin, J. Phys. Chem. **86**, 2294 (1982); L. Peliti and S. Leibler, Phys. Rev. Lett. **54**, 1690 (1985).

[20]S. F. Edwards, Proc. Phys. Soc. London **85**, 613 (1965).

[21]For review, see Y. Oono, in *Advances in Chemical Physics*, edited by I. Prigogine and S. A. Rice (Wiley, New York, 1981), Vol. LXI, p. 301.

[22]M. Fixman, J. Chem. Phys. **23**, 1656 (1955); J. des Cloizeaux, J. Phys. (Paris), Lett. **41**, L-151 (1980); J. Phys. (Paris) **42**, 635 (1981).

[23]M. E. Cates, Phys. Rev. Lett. **53**, 926 (1984); J. Phys. (Paris) **46**, 1059 (1985).

[24]J. Rudnick and G. Gaspari, J. Phys. A **19**, L191 (1986); J. A. Aronovitz and D. R. Nelson, J. Phys. (Paris) **47**, 1445 (1986), and references therein.

[25]P. E. Rouse, Jr., J. Chem. Phys. **21**, 1272 (1953).

[26]B. H. Zimm, J. Chem. Phys. **24**, 269 (1956).

[27]R. Orwoll and W. Stockmayer, Adv. Chem. Phys. **15**, 305 (1969).

[28]See, e.g., T. A. Witten, in *Physics of Finely Divided Matter*, edited by N. Boccara and M. Daoud (Springer, Berlin, 1985).

[29]F. Bueche, J. Chem. Phys. **22**, 603 (1953); A. Miyake, Prog. Theor. Phys. (Kyoto) Suppl. **10**, 56 (1959).

[30]P. G. de Gennes, Macromol. **9**, 587 (1976).

[31]P. G. de Gennes, J. Chem. Phys. **55**, 572 (1971).

[32]K. Kremer and K. Binder, J. Chem. Phys. **81**, 6381 (1984).

[33]R. C. Ball (private communication).

[34]A similar experiment has been performed independently by M. A. F. Gomez [Universidade de Pernambuco, Recife, Brazil, (unpublished)], who obtained analogous results for thick surfaces, and larger d_f for thin surfaces (possibly a crossover effect). We are grateful to B. B. Mandelbrot for bringing this work to our attention.

[35]The simple Flory argument preceding Eq. (3.3) runs into conceptual problems for $D > 2$, since R_G^2 of a phantom surface becomes independent of L. Nevertheless, we expect the argument following Eq. (3.3) and the relation (6.1) to remain valid even in that region, since they directly access the interacting fixed point.

[36]See, for example, papers cited in Thin Solid Films, **68** (1980); **99** (1983).

[37]J. H. Fendler and P. Tundo, Acc. Chem. Res. **17**, 3 (1984).

[38]R. Zallen, *The Physics of Amorphous Solids* (Wiley, New York, 1983), Chap. 3.

[39]D. Turnbull (private communication). See also, M. J. Aziz, E. Nygren, J. F. Hays, and D. Turnbull, J. Appl. Phys. **57**, 2233 (1985).

[40]P. Pfeuty, R. M. Velasco, and P. G. de Gennes, J. Phys. (Paris) Lett. **38**, L-5 (1977).

[41]Details of the calculation will be given elsewhere.

[42]B. B. Mandelbrot, in *Turbulence and the Navier-Stokes Equation*, Vol. 565 of *Lecture Notes in Mathematics*, edited by R. Teman (Springer, Berlin, 1976), p. 121.

[43]U. Frisch, P.-L. Sulem, and M. Nelkin, J. Fluid. Mech. **57**, 719 (1978).

[44]P. G. Saffman, in *Topics in Nonlinear Physics*, edited by N. J. Zabusky (Springer, New York, 1968), p. 485. See also, P. Moin and J. Kim, J. Fluid Mech. **155**, 441 (1985).

[45]D. R. Nelson, Phys. Rev. B **18**, 2318 (1978).